

ARP 194: EVIDENCE OF TIDAL STRIPPING OF GAS AND CROSS-FUELING

P. Marziani¹, D. Dultzin-Hacyan², M. D’Onofrio³, J. W. Sulentic⁴**ABSTRACT**

We present new imaging and spectroscopic observations of the interacting system Arp 194 (\equiv UGC 06945 \equiv VV 126). The northern component (A194N) is a distorted spiral or ring galaxy likely disrupted by a collision or close encounter with a southern galaxy (A194S). There is evidence that a third galaxy with similar recession velocity is projected on A194N but its role is likely secondary. A194S is connected to A194N by a string of emission knots which motivates our interpretation that the former was the intruder. Three of the knots are easily discernible in B,R, and $H\alpha$ images and are assumed to trace the path of the intruder following the encounter, which we estimate occurred a few 10^8 yr ago.

Both A194S and N are experiencing strong bursts of star formation: the $H\alpha$ luminosity indicates a total star formation rate $\sim 10 M_{\odot}\text{yr}^{-1}$. The lack of detectable J and K emission from the blobs, along with strong $H\alpha$ emission, indicates that an evolved stellar population is not likely to be present. The brightest knot (closest to A194S) shows a star formation rate of $\approx 1.2 M_{\odot}\text{yr}^{-1}$ which, if sustained over a time $\approx 7 \times 10^7$ yr, could explain the spectral energy distribution. This suggests that the stripped matter was originally predominantly gaseous. The brightest knot is detected as a FIRST radio source and this is likely the signature of supernova remnants related to enhanced star formation. Motions in the gas between the brightest knot and A194S, traced by an emission line link of increasing radial velocity, suggests infall toward the center of the intruder. Arp 194 is therefore one of the few galaxies where evidence of “cross-fueling” is observed.

Subject headings: galaxies: individual (Arp 194) – galaxies:interactions – galaxies: kinematics & dynamics – galaxies: nuclei – galaxies: starburst

¹Osservatorio Astronomico di Padova, INAF, vicolo dell’Osservatorio 5, I-35122 Padova, Italy; marziani@pd.astro.it

²Instituto de Astronomía, UNAM, México, D. F. 04510, México; deborah@astrocu.unam.mx

³Dipartimento di Astronomia, Università di Padova, Vicolo dell’Osservatorio 3, I-35122 Padova, Italy; donofrio@pd.astro.it

⁴Department of Physics and Astronomy, University of Alabama, Tuscaloosa, AL 35487, USA; giacom@merlot.astr.ua.edu

1. Introduction

Arp 194 (Arp 1966; \equiv UGC 06945 \equiv VV 126; Vorontsov-Vel’Yaminov 1977) is a small-angular-size system of two major components: a north-western galaxy of disrupted morphology ($0'.8 \times 0'.6$; see Fig. 1 and Fig. 2), and an apparently more regular galaxy ($0'.35 \times 0'.35$) located ≈ 40 arcsec to the South-East. From the heliocentric velocity of the Arp 194S (\equiv A194S hereafter), $v_r \approx 10500$ km s $^{-1}$ (see §3), we infer a distance of 175 Mpc for the system ($H_0 \approx 60$ km s $^{-1}$ Mpc $^{-1}$). Arp 194N and Arp 194S are therefore separated by a projected linear distance $d_p \approx 34$ Kpc (1 arcsec corresponds to $d_p \approx 850$ pc). Arp described the Arp 194 system as belonging to the class of “galaxies with material ejected from nuclei.” Arp noted further “outer material connected by thin filament to very hard nucleus.” Several peculiar features of Arp 194N (\equiv A194N) have been also discussed in an early study (Metlov 1980).

Theoretical modeling involving a reliable treatment of dissipative phenomena like star formation, as well as high resolution numerical simulations of stellar and gas motions are still the current frontier in our understanding of interacting galaxies (see e.g., Hearn & Lamb 2001; Semelin & Combes 2000; Barnes & Hernquist 1998; Barnes & Hernquist 1996; Mihos & Hernquist 1996). From simulations, we expect a wide range of phenomenological properties due to interaction. Gravitational forces can marginally enhance the star formation rate (SFR) in an unbound intergalactic encounter as well as give rise to the most luminous bursts of star formation observed in merging systems (see e.g., Krongold et al. 2002, and references therein). Tidal effects drive noncircular motion in disk galaxies, can strip a significant amount of stars and gas, and even lead to the formation of the so-called tidal-dwarf galaxies (Barnes & Hernquist 1992). A related issue is the role of gravitational interaction in fueling nonthermal nuclear activity. Both simulations and observations of single interacting systems are a necessary complement to statistical studies on the frequency of interacting systems among active galaxies, since the latter provide valuable but only circumstantial evidence in favor of interaction as a major driver of nuclear activity (Krongold et al. 2002; see however Schmitt 2001, and references therein). Collisional ring galaxies are excellent laboratories for studying galactic evolution, global star formation, and the occurrence of gas cross-fueling among galaxies. The prototype of this class of objects is the Cartwheel galaxy A0035-33. Only few systems similar to this object are known: among the best studied we recall VII Zw 466, Arp 10, II Zw 28, II Hz 4, Abell 76, LT 36, NGC 985, LT 41 (Appleton & Marston 1997). Other likely cases are Arp 119 (Hearn & Lamb, 2001), Arp 118 (Charmandaris et al. 2001), Arp 284 (Smith & Wallin 1992, Smith et al. 1997), and Arp 143 (Appleton et al. 1992). The dominant ring morphology is thought to result from a head-on collision between two galaxies, one of which traveled close to the spin axis of the other, striking the disk close to its center. The resulting gravitational perturbation is believed to drive a set of symmetrical waves or caustics through the stellar disk (Lynds & Toomre 1976, Theys & Spiegel 1976, Toomre 1978, Appleton & Struck-Marcell 1987, Struck-Marcell 1990). Computer simulations of such head-on encounters, in which at least one galaxy has a significant gaseous component, show indeed the production of density enhancements and shock waves in the interstellar medium. These high density regions coincide with the location of recent, large scale

star formation observed in ring galaxies.

Fig. 1 and Fig. 2 suggest that A194N is a collisionally induced ring galaxy connected to the past intruder A194S by a string of relatively bright knots (§3). Several photometric properties indicate star formation rates typical of Starburst galaxies (§3.5). The surprisingly strong radio emission from A194S and knot A is likely due mainly to supernova remnants which imply even higher star formation rates (§3.5.1) and substantial internal obscuration. Relatively rare systems like Arp 194 where gas motions are induced by a head-on encounter enable us to unambiguously infer the geometry of the system. In this case that information provides evidence for “cross-fueling” (see §4.1). Our results for Arp 194 have intriguing implications on the analysis and interpretation of galactic superwinds (§4).

2. Observations, Data Reduction & Analysis

Johnson (B, R) and narrow band ($H\alpha$) images of Arp 194 were obtained at the Cassegrain focus of the 2.1 m telescope of the Observatorio Astrónomico Nacional of México at San Pedro Martir (SPM) on January 30–31, 1995. The detector was a Tektronik CCD (24 μm square pixel size, 1024 \times 1024 format) that yielded a scale of 0.315” pixel $^{-1}$, and a field of view of 5.4’. A narrow band filter with $\lambda_C \approx 6819 \text{ \AA}$, and $\Delta\lambda \approx 86 \text{ \AA}$ allowed coverage of the $H\alpha + [\text{NII}]\lambda\lambda 6548, 6583$ blend of Arp 194 (§3.1). Table 1 provides a log of each single exposure taken at SPM.

Long slit spectra were obtained on February 2, 1995 at the 2.1 m telescope equipped with a Boller & Chivens spectrograph. A 1200 lines mm^{-1} grating was employed for observations of the $H\alpha$ spectral region (coverage $\approx 6170 - 7240 \text{ \AA}$). Four spectrograms were taken, two at position angle P. A. $\approx 145^\circ$ and two P. A. $\approx 118^\circ$, with an exposure time totaling 60 min. at each P. A. (see Fig. 1 for slit placement). The slit was opened to 200 μm (2.6” on the focal plane of the telescope). This setup resulted in a resolution of $\approx 2.5 \text{ \AA}$ FWHM ($\approx 110 \text{ km s}^{-1}$ at redshifted $H\alpha$). The data reduction for both imaging and spectroscopic data and the calibration procedure followed standard IRAF practice and has been identical to that employed by Marziani et al. (1999), who used data obtained during the same nights. We will not describe them again here. Table 3 presents line fluxes for emission line regions isolated along the slit.

3. Results

3.1. Morphology & Photometry

The morphology of the Arp 194 system in the B band is shown in Fig. 1, where some of the most prominent features are identified. A multifrequency view is provided in Fig. 2. The four panels show (clockwise from top left) the SPM B-band image (with a cut optimized to show the internal structure at the expense of loss of the fainter envelope), the continuum subtracted $H\alpha +$

[NII] $\lambda\lambda 6548,6583$ narrow band image, the B–R color index map, and the radio map at 1.4 GHz obtained from the FIRST survey (Becker et al. 1995). Table 2 reports the photometric properties of the main features visible in these maps. The uncertainty in the B and R photometry is estimated to be $\approx \pm 0.05$ mag at a 2σ confidence level. B–R values are therefore accurate within $\lesssim 0.1$ mag. The uncertainty associated to the overall H α + [NII] $\lambda\lambda 6548,6583$ calibration is estimated to be within 10 %. Due to the diffuse nature of large part of H α emission, an appropriate uncertainty is probably a factor 2 for the measurements on the faintest and most diffuse regions, while it should be within 20 % for the brightest and least diffuse ones. A194S is a surprisingly strong radio source when compared to nearby Seyfert galaxies. The specific power of A194S is $\log P_{\nu,1.4\text{GHz}} \approx 22.1$, with $P_{\nu,1.4\text{GHz}}$ in W Hz^{-1}), placing it at the high end of the distribution of radio power in Palomar Seyferts, which cover the range $\log P_{\nu,1.4\text{GHz}} \approx 18\text{--}22$ (Ulvestad & Ho 2001; Ho & Ulvestad 2001). Of course this is still negligible compared to nearby radio galaxies such as NGC 1275 with $\log \nu P_{\nu,1.4\text{GHz}} \approx 25.6$ (Owen et al. 1980).

Another remarkable feature of this system is a string of relatively bright knots (“blobs”) in between the two components of Arp 194, aligned along the north western direction (the “streamers” in the terminology of Metlov 1980). The blobs B and C have B–R ≈ 0.12 and 0.26 respectively. In Table 5, the J and K magnitudes are upper limits from the isophotal contours published by Bushouse & Stanford (1992). The blobs are not present at the lowest contour levels traced by these authors. The trail of blobs between A194S and A194N can be readily interpreted as stripped gas due to the interpenetrating encounter between A194S and A194N (see Marziani et al. 1994; Horellou & Combes 2000). There are several lines of evidence in favor of this interpretation:

- the rough alignment of the three main blobs observed in between A194S and A194N. The blobs literally provide a trail of “footprints” tracing the path of the intruding galaxy (A194S) after crossing A194N. They identify a direction pointing close to the geometrical center of A194N;
- the lack of any K counterpart for all blobs, which suggests a common origin for the blobs. In particular, it rules out that blob A is a background galaxy;
- almost no solution of continuity nor any radial velocity discontinuity H α emission in the 2D spectra at P. A. 145° (see Fig. 3 and §3.3);
- several features of A194N, which can be ascribed to a collisional ring, as discussed below.

Following the collision interpretation we might expect Arp194 to show features predicted by models for off-center interpenetrating encounters including: (1) a prominent outer ring and (2) displacement of mass toward the ring (Gerber et al. 1992; see also the K images of several ring galaxies in Appleton & Marston 1997). A194N can be interpreted as a distorted ring galaxy although tracing the outer ring is not easy. Two arcs towards the south and north can be traced unambiguously, suggesting a ring of radius $R_d \approx 17$ Kpc. The hollow region towards the SE

reinforces the collisional ring galaxy interpretation because it cannot be easily explained in other terms. Another supporting element involves the trend in radial velocities along P.A.=145°, which can be more easily explained as the result of expansion than rotation (see §3.3). A194S shows a larger and brighter nuclear bulge suggesting that it is an earlier morphological type (Sa-Sb?) than N (originally type Sc?). Two blue arc-like features (Fig. 1 & Fig. 2) are displaced towards the eastern and western sides of the A194S nucleus (see also the color map). They may be signatures of a ring-like expansion wave produced by the assumed head on encounter between A194N and S.

Interpretation of A194N is complicated by the complex morphology on the north-western side. Two main condensations (corresponding roughly to A194N-A and A194N-B) are visible in the K images. This may indicate that we are detecting the nucleus of N and another galaxy projected nearby (i.e. A194N + an additional perturber). The color map reddest region to the North ($B - V \gtrsim 1$) may be associated to such a perturber. The issue requires more data but the trail of blobs suggests that A194N and S are the main players in this interaction. Our discussion reflects that assumption.

3.2. Emitting Regions

The Nucleus of A194S \equiv A194S-A The intruder nucleus is a luminous H α source ($L(\text{H}\alpha) \approx 2 \times 10^{41}$ ergs s $^{-1}$) with color index B–R \approx 0.5. The ratio $I([\text{N II}]\lambda 6584)/I(\text{H}\alpha) \approx 0.4$ (Fig. 5 and 4) suggests that there is no significant source of ionization other than hot stars. The moderate $I([\text{S II}]\lambda\lambda 6716, 6731)/I(\text{H}\alpha)$ ratio (≈ 0.3) and very low $I([\text{O I}]\lambda 6300)/I(\text{H}\alpha)$ ratio (≈ 0.02) support this conclusion. A further confirmation comes from the $I([\text{O III}]\lambda 5007)/I(\text{H}\beta)$ ratio (≈ 0.8) measured by Metlov (1980). Line ratio diagnostic diagrams (Veilleux & Osterbrock 1987) show that A194S is located very close to the HII zone. Our data show no evidence for non-thermal nuclear activity. In this respect, it is worth noting that there is (Fig 4) no variation of the $I(\text{H}\alpha)/I([\text{N II}]\lambda\lambda 6548, 6583)$ ratio along the slit (an increase would be expected if a nonthermal contribution were present). The ratio $I(\text{H}\alpha)/I(\text{H}\beta)$ measured by Metlov (1980) 3.7:1.0 suggests moderate extinction ($E(B - V) \approx 0.2$). The heliocentric $v_r \approx 10502$ km s $^{-1}$ agrees with Metlov’s (1980) determination within 10 km s $^{-1}$.

Blob A This is the second strongest source of H α emission in the interacting pair and it is also clearly detected as a FIRST radio continuum source. Metlov (1980) measured $I([\text{O III}]\lambda 5007)/I(\text{H}\beta) \approx 1.56$. The intensity ratios $I([\text{N II}]\lambda 6583)/I(\text{H}\alpha) \approx 0.23$, $I([\text{S II}]\lambda\lambda 6716, 6731)/I(\text{H}\alpha) \approx 0.24$, and $I([\text{O I}]\lambda 6300)/I(\text{H}\alpha) \approx 0.027$ indicate that HII emission is dominant and this is confirmed by the source location in the diagrams of Veilleux & Osterbrock (1987). A ratio $L(\text{H}\alpha)/\nu P_{1.4\text{GHz}} \approx 800$ is a useful measure of what can be inferred about star formation processes. It is noteworthy that Blob A is clearly connected to the nucleus of A194S by more extended line emission (Fig. 3; see §3.3).

A194N-A Source A194N-A is likely to be the nucleus of the disrupted spiral but it was only partially in the slit at both position angles. $H\alpha$ and $[\text{NII}]\lambda\lambda 6548,6583$ show $\text{FWHM} \approx 250 \text{ km s}^{-1}$ which is approximately twice as broad as the adjacent emitting regions. The observed broadening is significant at a confidence level $\gtrsim 3 \sigma$ taking into account a FWHM error of 15% or $\approx 30 \text{ km s}^{-1}(1\sigma)$. The broadening is appreciable in both spectra and it is due to the presence of an additional (redshifted) line component in the slit since the $H\alpha$ and $[\text{NII}]\lambda\lambda 6548,6583$ profiles are double-peaked with peak $\Delta v_r \approx 130 \text{ km s}^{-1}$ (see Fig. 5, where spectra of the main emitting regions are shown). The $I([\text{NII}]\lambda\lambda 6548,6583)/I(H\alpha)$ ratio (≈ 0.6) for the red component suggests the presence of non-thermal emission probably associated with shock-heated gas (not strong, otherwise the $[\text{SII}]\lambda\lambda 6716,6731$ lines would be detected).

3.3. Radial Velocity Curves

Fig. 3 is a grey-scale reproduction of the extended $H\alpha + [\text{NII}]\lambda\lambda 6548,6583$ emission. The radial velocity (v_r) curve derived from this figure is shown in Fig. 6 (centered on A194S-A) and in Fig. 7 at P. A. $\approx 118^\circ$. Both radial velocity curves agree qualitatively with the data provided by Metlov (1980). Emission is continuous between blob A and A194S. v_r increases monotonically to within $\approx 3''$ NW of A194S-A (maximum $\Delta v_r \approx 120 \text{ km s}^{-1}$). This emission line component produces the cusp in the radial velocity curve between 0–5'' from the continuum peak of A194S. The velocity curve on the northern side of A194S is obviously not due to rotational motion because it appears to turn over. The velocity cusp is most likely due to blending of the rotational velocity field with the redward-displaced component visible in Fig. 3. This is made more evident by the contour overlaid on Fig. 3 and by the cross-dispersion intensity profile shown in the upper panel of Fig. 4. The main $H\alpha$ component has been summed over $-160 \text{ km s}^{-1} \lesssim \Delta v_r \lesssim 110 \text{ km s}^{-1}$; the redward component in the range $110 \text{ km s}^{-1} \lesssim \Delta v_r \lesssim 330 \text{ km s}^{-1}$. In correspondence of $\Delta d'' \approx 4''$, the total $H\alpha$ emission is significantly broader since the two $H\alpha$ components are blending together (the $H\alpha$ profile appears double-peaked).

3.4. The Geometry and Kinematics of the Encounter

Any inferences on the systemic v_r of A194N-A are uncertain (§3.2). The P.A. = 145° slit, however, crosses A194N not far from the geometrical center of the ring. Our spectrum at PA = 145° mainly samples the “empty” inner region of A194N. This gives us confidence that we are measuring a reasonably reliable radial velocity $v_{r,N}$ for A194N at $\approx 41''$ in Fig. 6 (the edges of the ring are at $30''$ and $50''$, and interestingly, in their correspondence the v_r is constant over $3''$). A fit to the v_r curve in this region is shown by a filled thin line in Fig. 6. We derive a value $v_{r,N} \approx 10477 \text{ km s}^{-1}$ if we consider the midpoint between the two segments of constant v_r ; $v_{r,N} \approx 10457 \text{ km s}^{-1}$ if we consider the average v_r between the two segment. The roughly symmetric appearance of the radial velocity curve around this point reinforces our confidence that $v_{r,N} \lesssim 10500 \text{ km s}^{-1}$. We

derive from the observed continuum peak (the 0 point of Fig. 6) $v_{r,S} \gtrsim 10502 \text{ km s}^{-1}$. Therefore, A194S is receding from A194N with $\Delta v_{r,\text{coll}} \approx 25 - 40 \text{ km s}^{-1}$.

We conclude that A194S is more distant and this implies that the motion of the blobs relative to it follows straightforwardly. Blob A, in the 2D spectrum of Fig. 3 is connected to the emission line component of increasing v_r detected up to a few arcsecs from the continuum peak. The Δv_r between A194S-A (v_r measured at continuum peak) and blob is still positive ($\Delta v_r \approx 30 \text{ km s}^{-1}$). Therefore, blob A cannot be the product of outflow for the obvious reason that it would be moving in the wrong direction. *If the blobs trail A194S, Blob A – as well as the extended emitting gas of increasing v_r in between blob A and A194S-A – must be falling toward A194S-A.* The validity of this results is based on two considerations: (1) the blobs, and blobs A especially, trail after A194S; (2) $\Delta v_{r,\text{coll}} \gtrsim 0 \text{ km s}^{-1}$, implying that A194S is further from us than A194N. In this case, blob A is closer to us than A194S. We must remark that, albeit $\Delta v_{r,\text{coll}}$ is small, $\Delta v_{r,\text{coll}} \lesssim 0 \text{ km s}^{-1}$ is inconsistent with the v_r curve and the geometry of the system (see Fig. 6).

Ring Age and Time After Crossing To estimate the time after crossing, we can consider that, in the special case of a head-on encounter in which the direction of motion of the intruder is strictly perpendicular to the plane of the target galaxy, the distance between the intruder and the target galaxy can be deprojected once the inclination of the target galaxy is known (this may not be strictly true for Arp 194; this is just a first approximation). The main underlying assumption is that the ring starts to expand at the time the intruder nucleus was interpenetrating the disk of the target, as suggested by theory and numerical simulations (Lynds and Toomre 1977). The expansion velocity will be $v_{exp} = R_d/d_p \Delta v_r \tan i \approx 25 \Delta v_{r,\text{coll},50} \tan i \text{ km s}^{-1}$. The time after crossing is $\tau = R_d/v_{exp}$. We can estimate the inclination of the ring making two extreme choices: (1) the NW end is traced by the Arc Spots A,B,C; (2) the NW end is the fainter spot $\approx 5''$ to the NW from the Arc. Since this implies $54^\circ \lesssim i \lesssim 75^\circ$, we obtain $2 \times 10^8 \text{ yr} \lesssim \tau \lesssim 6 \times 10^8 \text{ yr}$ if $\Delta v_{r,\text{coll}} = 40 \text{ km s}^{-1}$. If $i = 64.5^\circ$, $\tau \approx 4 \times 10^8 \text{ yr}$.

3.5. Star Formation Properties

The total $\text{H}\alpha$ luminosity of the Arp 194 system is $\approx 1.5 \times 10^{42} \text{ ergs s}^{-1}$. This yields a star formation rate $\approx 10 \text{ M}_\odot \text{ yr}^{-1}$ for masses between 0.1 and 100 M_\odot , assuming a Salpeter Initial Mass Function (see Kennicutt 1998 for relationships and references). This value is comparable to the one of powerful Starburst galaxies.⁵ It is interesting to note that if we consider the tight FIR-radio correlation of star-forming systems (Mirabel & Sanders 1996), with logarithmic index $q=2.35$, $\log L_{\text{FIR}} \approx 14.92 \log P_\nu$, we obtain $L_{\text{FIR}} \approx 2.3 \times 10^{44} \text{ ergs s}^{-1} \approx 6 \times 10^{10} L_\odot$. Arp 194 may be well a luminous IRAS galaxy. A vigorous star formation going on in the produced ring

⁵Unfortunately, Arp 194 has not been covered by IRAS observations.

seems to be a common property of ring galaxies (Marston & Appleton 1995). Optical images often show a compact off-centered nucleus surrounded by a number of blue knots that are HII regions. The ring component often hosts giant molecular complexes, and its color is consistent with a very young stellar population. Indeed, the ring arcs of A194N stand out in the color map since they are bluer than the surrounding regions.

Is it just a Starburst? A Starburst surrounding the nuclear region, as well as infall of gas from above the galactic plane may produce extinction to the point to fully obscure an active galactic nucleus (AGN). Actually, the early stages in the life of an AGN may be dominated by obscuration, so that even the very AGN detection may be troublesome. This seems to be true over a wide range of luminosity, from ultra-luminous far IR galaxies ($L_{\text{FIR}} \sim 10^{12}L_{\odot}$), down to the nearest Seyfert 2 (see e.g., Krongold et al. 2002; Maiolino et al. 2000; Dultzin-Hacyan 1995; Sanders et al. 1988). We computed the $L(\text{H}\alpha)/\nu P_{\nu}$ at $\nu = 1.4$ GHz as a function of the aperture radius for increasing apertures from 2" to 9". In this interval the ratio is $L(\text{H}\alpha)/\nu P_{\nu} \approx 2200$, with a ± 10 % change along different aperture sizes. The nuclear value is larger than the value observed on Blob A (see below). Blob A is not strictly a galaxy and most likely lacks the deep potential well associated to the nuclei of galaxies where massive black holes are thought to be present. Furthermore, both the nucleus and blob A obey to the correlation between $f(\text{H}\alpha+[\text{NII}]\lambda\lambda 6548,6583)$ and radio f_{ν} at 20 cm found by Kennicutt (1983) for spiral galaxy, which implies $f(\text{H}\alpha+[\text{NII}]\lambda\lambda 6548,6583)/\nu f_{\nu} \approx 1500$. This suggests no contribution from an obscured active galactic nucleus in A194S-A.

Having ascertained that most of the $\text{H}\alpha$ and radio emission is due to HII regions, we can deduce several parameters related to star formation reported in Table 4. We will focus on blob A and B for which we have a more complete dataset. The absence of any J, and K counterparts for the blobs (Bushouse & Stanford 1992) readily suggests that, if the blob are associated to star forming regions, their age must be relatively young, and that mainly gaseous matter has been stripped through the encounter.

“First Generation” of Stars in Blob A? If we were observing a very young population (i.e., a first generation of stars in which *all* stars are still in the main sequence with a total mass reported in Col. 7 of Table 4), radio emission should be due exclusively to thermal Bremsstrahlung in the HII regions. In this case, the emissivity ratio between $\text{H}\alpha$ and radio specific flux is dependent only on the electron temperature T_e (Osterbrock 1989, pp. 80, 88, 95). Assuming $T_e \approx 10^4\text{K}$, we obtain that the expected ratio at $\nu = 1.4$ GHz is $j_{\text{H}\alpha}/\nu j_{\nu} \approx 44000$ for optically thin free-free emission. This value is most likely an underestimate because the emitting region should be optically thick at 1.4 GHz: HII regions have frequently a turnover frequency between the optically thick and thin regime at ≈ 3 GHz. Since the observed ratio is more than an order of magnitude smaller, we conclude that radio emission must be mainly due to a non-thermal sources associated to supernovae. The “first generation” scenario is not supported by the optical properties either. We computed the numbers of ionizing photons needed to sustain the $L(\text{H}\alpha)$, and hence the number of OB stars (spectral type

earlier than B9) under the assumption that no photon escapes from the nebulae. Approximately 30000 OB stars are needed for blob A. However, a larger number of OB stars would be needed to account for the B absolute magnitude ($M_{B, \text{blobA}} \approx -17.9$), implying that star formation has been going on beyond the main sequence lifetime of OB stars. Population synthesis calculations using STARBURST99 (Leitherer et al. 1999) confirm this suggestion. In Fig. 8, the dot-dashed line shows the spectral energy distribution expected for a star cluster of total mass $5 \times 10^6 M_{\odot}$, with a Salpeter IMF predicted by STARBURST99. Emission from such star cluster fails to reproduce the observed luminosity of blob A.

Population Synthesis We simulated blob A and blob B as star forming systems with $\text{SFR} \approx 1.22 M_{\odot} \text{yr}^{-1}$ and $\text{SFR} \approx 0.42 M_{\odot} \text{yr}^{-1}$ respectively (estimated from $L(\text{H}\alpha)$ and as reported in Table 4), using STARBURST99. In Fig. 8 we plot the luminosity in the bands for which we have available data (uncorrected for internal extinction), along with the results of STARBURST99 simulations (solid lines). A reasonable fit to the observed colors and to the absolute B magnitude of blob A is obtained for constant star formation rate and an age of 7×10^7 yr. This implies that the mass of the blob is $M_{\text{blobA}} \gtrsim 10^8 M_{\odot}$ (a lower limit since we do not know how much of gas mass belongs to the blob). We are able to reproduce the total blob A luminosity within a Starburst age significantly lower than the time lapsed after A194S and N crossing. Not surprisingly, this is not possible for A194S-A, the nucleus of A194S: if $\text{SFR}_{\text{A194S-A}} \approx 1.55 M_{\odot} \text{yr}^{-1}$, after 7×10^7 yr a star forming system would be less luminous than A194S by a factor ≈ 10 in the K band. This implies that *the tidally stripped matter making blob A was, in origin, predominantly gaseous.*

3.5.1. The Supernova Rate From Radio Properties : Evidence of Substantial Obscuration

Radio emission in star forming galaxies is expected from three major sources: (1) radio supernovæ (RSNæ), (2) supernova remnants (SNRs), and (3) cosmic ray electrons injected through the Fermi acceleration mechanism in the interstellar medium (see, e.g., Condon 1992 for an excellent review). We can write the emitted power as a function of time as $P = \sum_k \int_{t_{\text{min},k}}^{t_{\text{max},k}} dn(t)/dt P_k(t) dt$, where the integration is summed over the three main radio emission mechanisms, and $dn(t)/dt$ is the number of supernovæ per year, and we assume that the age of the starburst is longer than the maximum $t_{\text{max}} \sim 10^7$ yr (see below).

A notable example of radio-emitting supernova has been the RSN (with a type Ibc progenitor) discovered in the circumnuclear starburst region of NGC 7469, a Seyfert 1 galaxy (Colina et al. 2001). The conditions of NGC 7469 may be ultimately similar to the ones of A194S-A. However, unless a Starburst is extremely young, RSNæ due to type II events should dominate the radio luminosity contribution due to SNaæ. We consider as representative one of the best studied cases, SN 1979c in M100. The luminosity is an order of magnitude less than RSN NGC 7469, $\nu P_{\nu} \approx 5 \times 10^{36} \text{ergs s}^{-1}$, and the light curve can be modeled as flat for a time $t_{\text{max},1} \approx 2$ yr with a sharp rise and steep decline (see also Yin & Heeshen 1991; Mioduszewski et al. 2001). This seems to

be, at present, a reasonable albeit rough assumption. The contribution due to SNR, $P_{\nu, \text{SNR}}$ is a strong function of time. The SNR diameter depends on time as $D = 4.3 \times 10^{-11} (E_0/n_{e, \text{int}})^{\frac{1}{5}} t^{\frac{2}{5}}$, where D is in pc and t in years (Clark & Caswell 1976; see e.g., Ulvestad 1982) up to a $t_{\text{max}, 2} \approx 10^5$ yr. E_0 is the total energy of a SN, and $n_{e, \text{int}}$ is the electron density of the circumstellar medium ($n_{e, \text{int}} \sim 1 \text{ cm}^{-3}$). It is usually assumed that $E_0/n_e \sim 10^{51}$ ergs cm^3 . We consider the observational surface brightness Σ vs. D relationship in the form $\Sigma \approx 10^{-15} D^{-3} \text{ W m}^{-2} \text{ Hz}^{-1} \text{ sr}^{-1}$ (Ulvestad 1982, and references therein). Assuming a power law index 0.8 typical of type II SNaE (Weiler et al. 1986; Colina et al. 2001, and references therein), we obtain that the total power emitted at 1.4 GHz by a SNR as a function of time is $\nu P_{\nu, 1.4, \text{SNR}} \approx 1.3 \times 10^{35} t^{-\frac{2}{5}}$ ergs s^{-1} . A third term is due to relativistic electrons injected by supernova shocks in the interstellar medium. These “cosmic ray” electrons are thought to account for $f = 90\% - 94\%$ of the total radio power output from a supernova remnant (Condon 1992; Bressan et al. 2002), and may radiate for $t_{\text{max}, 3} \lesssim 10^7$ yr.

Assuming $dn(t)/dt$ independent on time, we obtain a rate $dn/dt \sim 2 \cdot (1 - f) \sim 0.1 - 0.2$ SNæ yr^{-1} for the nuclear region, and $\sim 1 \cdot (1 - f) \approx 0.05 - 0.1$ SNæ yr^{-1} for blob A. The SN rate deduced from radio power is in any case much larger than the value expected from stellar population synthesis, which predicts $dn(t)/dt \approx 0.015$ SNæ yr^{-1} for the nuclear regions of A194S, and $dn(t)/dt \approx 0.01$ SNæ yr^{-1} for blob A. The SN rate deduced from radio is $\sim 5 - 10$ times larger than the SN rate deduced from optical properties. This hints at (1) the presence of an AGN, which may significantly affect the total power of A194S; however, this does not seem the case since the ratio between optical and radio SN rate on A194S-A is similar to that of blob A; at (2) obscuration; (3) a short-lived ($\sim 10^7$ yr), post-Starburst phase in which the ratio $\text{SFR}/\nu P_{\nu}$ reaches a minimum (Bressan et al. 2002). This is predicted for an impulsive Starburst, and is due to the strong enhancement of the radio emission following the Supernova explosion of the lowest-mass type-II supernova progenitors (which are also the most frequent for standard IMFs). Obscuration is most likely to play the major role. Especially in systems like the nuclear regions of A194S, and blob A which are spheroidal in appearance, $\text{H}\alpha$ emission may be detected only from the star forming regions nearer to be observer. The SFR measured from the FIR luminosity is $\gtrsim 10$ times larger than the SFR measured from $\text{H}\alpha$ (Kennicutt 1998). The rate of SNæ found from a search in the K band is also a factor $\sim 5 - 10$ then the rate estimated from optical surveys (Maiolino et al. 2002; Mannucci et al. 2002, in preparation).

4. Discussion

4.1. Cross-Fueling in Interpenetrating Encounters

Numerical simulations of head-on collisions between galaxies show that a substantial mass of gas is “splashed out” into a bridge connecting the two centers of potential. After the collision, the gas is re-accreted either from the intruder and from the primary disk. The amount of material pushed out in the collision depends on the relative orientation and impact parameter of the en-

counter. The subsequent infall is spatially asymmetric and is primarily located in a well defined streams. Most of the accreted gas ends up in the central regions of the model galaxies (Struck 1997). However, cross-fueling is definitely not an easy phenomenon to prove observationally. In the framework of a galaxy pair, it implies three physical requirements: (1) that gas is stripped from one galaxy; (2) that the gas, stripped from one galaxy, is falling toward the other; (3) that the infalling gas is actually fueling a Starburst or an AGN. These three conditions may be met only in very special systems, and may be demonstrable in many fewer. At least, in the case of collisional ring galaxies systems like Arp 194 it is easy to test whether cross fueling is indeed occurring. First, the blob and the morphology of A194N provide evidence in favor of stripping. The second condition is also satisfied with reasonable certainty *for blob A* (nothing can be said on blob B and C). On blob A we are observing H α and [NII] $\lambda\lambda$ 6548,6583 line components whose redshift is increasing as the gas is approaching the nucleus of A194S. The third condition is also met, since the SFR \approx 4.5 M $_{\odot}$ yr $^{-1}$ for A194S-A and \sim 10M $_{\odot}$ yr $^{-1}$ are typical for estimates of SFR from H α luminosity in Starburst galaxies.

The emission line feature observed between blob A and A194S in the spectrum at P. A. =145 $^{\circ}$ is not unlike the one observed in NGC 7592, in which the two interacting galaxies are much closer, and in which a bright H α filament connects the nuclei of the two components (Rafanelli & Marziani 1992; Marziani et al. 2001). Interpenetrating encounters lead to some easily demonstrable cases of tidal stripping. At least two other cases have been studied in detail, Kar 29 and ESO 253-IG026 (Marziani et al. 2001, Marziani et al. 1994). ESO 253-IG026 shows an impressive, bright filament connecting the two galactic components. Evidence of cross-fueling has been collected in other galactic pairs, especially in mixed spiral/elliptical pairs in which a Starburst has been induced in the early type component: for example, in AM 0327-285 (de Mello et al. 1995; 1996), and in Arp 105 (Duc et al. 1997; see also Domingue 2001). We can study more easily some systems containing a collisional ring galaxy since they are at a special timing after contact and oriented favorably. Even if the conditions are special, they provide a laboratory to study accretion gas flows on 100 pc – Kpc scales which cannot be obtained as easily in more complex systems like most merging systems.

4.2. Tidal Stripping, Tidal Dwarf Galaxies & the Superwind Phenomenon

Albeit the blob B and C look slightly fainter than A, it is conceivable that they may be of comparable mass. The total mass of the blobs can therefore be several 10 8 M $_{\odot}$. The ejection of stellar and gaseous material into the intergalactic medium and its subsequent rearranging may lead ultimately to the formation of self-gravitating tidal dwarf galaxies (Duc et al. 2000). In this respect, it is interesting to note that the mass of blob A is within the range of dwarf galaxies.

The Arp 194 system shows that a part of the orbital energy can be transferred to the gas motion (e.g., Marziani et al. 1994 in the case of Kar 29, Horellou & Combes 2000) in the special case of a collisional ring galaxy. This is expected in general from simulations of interacting galaxies.

Orbital energy transfer leads to vertical motions of gas from a system that, when unperturbed, was dynamically very cold with a very low vertical velocity dispersion. Filamentary structures emerging from disk and dwarf galaxies are a telltale signature of superwinds (see for instance the spectacular case of NGC 1808; Phillips 1993). Superwinds are currently explained as due to the kinetic energy injected by stellar winds and SNæ around compact Starburst regions (e.g. Heckman et al. 1993; Heckman 2001). This explanation neglects the observational fact that the wide majority of superwind galaxies belong to strongly interacting systems (Marziani & Dultzin-Hacyan 2000). A rather large fraction of superwind galaxies (possibly 9 out of 20, of which 3 with obvious evidence of tidal stripping) were found in merging systems. Small companions, leading to appreciable perturbations, were also seen near $\approx \frac{1}{3}$ of the superwind galaxies. Also in the case of minor mergers, the velocity dispersion in the inner disk is expected to be significantly increased, and the disk structure to become unstable (Walker et al. 1996). Implications of ongoing interactions – and of gravitationally-induced, non-rotational gas motions – have not been taken into account in the theory of galactic superwinds. Even if it is possible to obtain a momentum and energy flow consistent with the observed superwind properties from the mass ejections by stellar wind and SNæ (Leitherer et al. 1992), several superwind aspects – including the possibility that the wind matter could escape from the galactic potential well – could be influenced if the out-of-disk flow is eased by tidal forces, since most superwind flows are apparently only “marginally bound” (Martin et al. 2000). There could be important consequences for the enrichment of any intra-cluster medium. We know the relative velocity between blob A and A194N-A. We can estimate the kinetic energy of tidally stripped matter as $E = \frac{1}{2}M_{\text{blob}}\Delta v^2 \approx 2.5 \times 10^{54}M_{\odot}\Delta v_{50}^2$ ergs. This is a lower limit, since the blob mass could well be much larger than estimated. The kinetic energy imparted to blob A corresponds to the total kinetic energy produced by $\sim 10^3 - 10^4$ SNæ, and it may be still a small fraction of the total superwind energy ($\sim 10^{55} - 10^{57}$ ergs, which corresponds to the total output of $10^4 - 10^6$ supernovæ). However, gravitational forces could have still an important impact. The kinetic energy could easily be much higher, since Δv imparted to the streaming gas could be much larger than the one assumed on the basis of the blob A observations. The kinetic energy value for tidally stripped matter and superwind outflow can therefore be comparable. We have shown that at least blob A and B can be thought as being entirely gaseous in origin. The relevance of Arp 194 to the superwind phenomenon is that it demonstrates observationally that gas motions can be perturbed to the point of giving rise to a stream perpendicular to the galactic plane because of gravitational acceleration.

There are other examples of a superwind-like outflow manifestly driven by interactions. Kar 29 is likely to be the result of a high velocity encounter ($\Delta v_r \approx 1000 \text{ km s}^{-1}$) between an early-type galaxy (the northern component) and a late-type spiral (see Hearn & Lamb 2001 for a review of observational data on this object). The stripped gas emerging from the spiral southern component has not been captured by the elliptical, and may be instead falling back toward the spiral as in a true “galactic fountain.” Fraternali et al. (2001) found that the “galactic fountain” HI motions in the spiral NGC 2403 are difficult to explain in the pure superwind scheme without accounting for interactions. Also, van der Hulst and Sancisi (1988) suggested that the high velocity HI gas moving

at high speed perpendicular to the disk of Messier 101 could be explained in term of a collision between a large gas mass and the disk of Messier 101 itself. Similarly, some high velocity clouds observed in our Galaxy are likely due to tidal effect related to the crossing of the Galaxy by the Large Magellanic Cloud (e.g., Wakker & van Woerden 1997). These findings can be understood through the simulations mentioned in the introduction. We conjecture that, in mergers and in minor mergers, there could be an important effect of gravitational forces on gas motion perpendicular to the original disk plane.

5. Conclusion

We have analyzed in detail the photometric properties and the kinematics of the strongly interacting system Arp 194. The main constituents of this system are a collisional ring system (A194N) and an intruder (A194S) that have experienced an interpenetrating, head-on encounter a few 10^8 yr ago. We have shown that tidally stripped gas is falling toward the center of the intruder, A194S, and that it is fueling a strong nuclear and circumnuclear Starburst. Arp 194 is therefore one of the few known objects for which convincing evidence of cross-fueling exists. Considering that gas is usually confined in a “dynamically cold” configuration in disk galaxies, the Arp 194 case indicates transfer of orbital energy to the internal motion of gas during the the encounter. We suggest that gas motions in superwind galaxies – which are mostly interacting systems – could also be affected by the same mechanism.

Several aspects of the Arp 194 system deserve further scrutiny. The morphology of A194N is fairly complex, and the distorted morphology of the ring as well as the bright arc of A194N indicate the possibility of perturbations by a third party. A full coverage with slit spectroscopy will allow to confirm the presence of a second intruder galaxy located approximately in correspondence of the northern side of the ring. High spatial resolution spectroscopy may reveal more complex motions in proximity of the nucleus of A194S. In the interacting galaxy pair NGC 1409/10, the ongoing mass transfer seems to follow a spiraling pattern (Keel 2000; similar considerations may apply to NGC 7592: Hattori et al. 2002). There is no indication of an hidden AGN presence from our data, but this result depends on the resolution of the FIRST survey data. It is possible that higher resolution data may reveal a high surface brightness compact core. In addition, further radio observations could detect radio supernova events: if $dn/dt \approx 0.3$, and if a radio supernova event remains detectable for ≈ 3 yr, we expect to reveal 1 event at any observing time.

P. M. acknowledges financial support from the Italian MURST through Cofin 00–02–004. D. D.- H. acknowledges grant IN 115599 PAPIIT-UNAM. We wish to thank Alessandro Bressan for providing us with the numbers of ionizing photons as a function of stellar spectral type and Radoslav Zamanov for a fruitful discussion on pulsars.

Table 1. Log of SPM Observations

Date-Obs	U.T. ^a	E.T. ^b [s]	P.A.	Filter/Sp. Range
30-Jan-1995	11 ^h 31 ^m	600	n. a.	R
30-Jan-1995	11 ^h 47 ^m	600	n. a.	R
30-Jan-1995	12 ^h 05 ^m	600	n. a.	R
30-Jan-1995	12 ^h 19 ^m	600	n. a.	R
30-Jan-1995	12 ^h 33 ^m	900	n. a.	H α + [NII]
30-Jan-1995	12 ^h 50 ^m	900	n. a.	H α + [NII]
30-Jan-1995	13 ^h 07 ^m	900	n. a.	H α + [NII]
31-Jan-1995	09 ^h 34 ^m	600	n. a.	R
31-Jan-1995	09 ^h 46 ^m	900	n. a.	B
31-Jan-1995	10 ^h 03 ^m	900	n. a.	B
31-Jan-1995	10 ^h 27 ^m	900	n. a.	B
2-Feb-1995	11 ^h 54 ^m	1800	145°	6165–7246 Å
2-Feb-1995	12 ^h 25 ^m	1800	145°	6165–7246 Å
2-Feb-1995	13 ^h 04 ^m	1800	118°	6165–7246 Å
2-Feb-1995	13 ^h 32 ^m	1800	118°	6165–7246 Å

^aUniversal Time at exposure start.

^bExposure Time duration in seconds for each single frame.

Table 2. Multifrequency Data for the Arp 194 System

Galaxy	Region Id.	$H\alpha + [\text{NII}]^a$ [ergs s ⁻¹ cm ⁻²]	B	R	B-R	J ^b	K ^b	$f_\nu(1.4 \text{ GHz})$ [mJy]
A194S	Total ^c	2.29E-13	15.17	14.39	0.78	14.22	12.67	$\gtrsim 5.35$
A194S	Nucleus ^e	7.94E-14	16.31	15.84	0.47	15.6	13.94	4.4 ^d
Arp 194	Blob A ^e	6.26E-14	18.34	17.87	0.47	$>18.35^f$	$>16.35^f$	2.79
Arp 194	Blob B ^e	2.17E-14	18.18	18.06	0.12	$>18.35^f$	$>16.35^f$...
Arp 194	Blob C	1.41E-14	17.98	17.72	0.26	$>18.35^f$	$>16.35^f$...
A194N	Total	1.38E-13	14.37	13.58	0.79	13.88	12.11	>0.40
A194N	A194N-A “Nucleus” ^e	$\lesssim 2.13\text{E-}14^g$	17.11	16.05	1.06	15.94	14.26	0.40
A194N	A194N-B	1.38E-14	17.51	16.34	1.17	15.51	13.62	...
A194N	Blob D	...	18.04	17.36	0.68
A194N	Arc Spot A	1.10E-14	18.25	17.87	0.38
A194N	Arc Spot B	7.14E-15	17.96	17.38	0.58
A194N	Arc Spot C	9.61E-15	18.03	17.15	0.88

^aThe [Nii] λ 6548 line falls right at the border of the employed narrow band filter; however considering that $I([\text{Nii}]\lambda 6583)/I(H\alpha) \approx 0.4$ almost everywhere, this implies that the $H\alpha + [\text{NII}]\lambda\lambda 6548, 6583$ fluxes should be corrected by $\lesssim 10\%$ (below our estimated uncertainties even for the brightest $H\alpha$ emitting regions). No correction was applied to the values reported in this Table.

^bNear Infrared photometry by Bushouse & Stanford (1992).

^cExcluding blobs.

^dValue measured on FIRST with an aperture of $5''.4$.

^eEmitting Region covered fully or in part with long slit spectroscopy (see Table 3).

^fRegions not visible in the isophotal contour map by Bushouse and Stanford (1992). The lower limit to the magnitude has been estimated from the lowest level isophote plotted by Bushouse and Stanford (1992), which are $\sigma \approx 20.5 \text{ mag arcsec}^2$ and $18.5 \text{ mag arcsec}^2$ for J and K band respectively. With a scale $1.35''/\text{pixel}$, the magnitude of a very faint object contoured in a square of 1 pixel of radius would lead to $m \approx -2.15 + \sigma$.

^g $H\alpha$ measured on a larger area than B and R.

Table 3. Emission Line Regions in Arp 194S

Galaxy	Region Id.	P. A. ($^{\circ}$)	v_{rHeI} [km s $^{-1}$]	[NII] λ 6548			H α			[NII] λ 6583			[SII] λ 6716			[SII] λ 6731		
				Flux ^a	W ^b	FWHM ^c	Flux ^a	W ^b	FWHM ^c	Flux ^a	W ^b	FWHM ^c	Flux ^a	W ^b	FWHM ^c	Flux ^a	W ^b	FWHM ^c
A194S	A Nucleus ^d	145	10502 \pm 3	8.4	24	170	64.5	170	170	26	68.5	170	11.9	33.6	220	8.4	24	200
A194	Blob A ^e	145	10532 \pm 7	1.2	...	140	15.6	...	\lesssim 110	3.61	...	110	2.1 ^f	...	200:	1.6
A194N	A “Nucleus” ^g	145	10435: ^h	0.46	5	250	0.27	3	250
A194N	A “Nucleus” ^g	118	10430 \pm 20	0.84	8.3	160	0.6	6.6	220

^aObserved flux in units of 10^{-15} ergs s $^{-1}$ cm $^{-2}$, uncorrected for redshift and internal extinction. Note that the correspondence between the long-slit emitting regions and the regions measured on the narrow and broad band images labeled with the same name is rather rough (it can be checked in Fig. 1 where the slit position is marked).

^bEquivalent width in \AA .

^cFull Width at Half Maximum in km s $^{-1}$ corrected for instrumental broadening $\approx 2.5 \text{\AA}$ FWHM.

^dOnly on this region a test on the accuracy of the spectra flux calibration can be done comparing the flux of the nucleus of A194S with the H α flux measured in the narrow band image (Tab. 5), since the summation was done on an area of similar value value ($\approx 25 \text{ arcsec}^2$). The agreement is very good even if the apertures are of different shape.

^eAlmost no continuum; equivalent width not defined.

^fFlux estimated from peak intensity ratio since the line profile is contaminated by a blemish.

^gOnly partially in the slit.

^hDouble-peaked H α and [NII] $\lambda\lambda$ 6548,6583 lines. A second component, partially resolved, peaks at $v_{\text{rHeI}} \approx 10566 \text{ km s}^{-1}$.

Table 4. Star Formation Results for the Arp 194 System

Galaxy	Region Id.	M_B^a	L(H α) [ergs s $^{-1}$]	SFR b [M $_{\odot}$ yr $^{-1}$]	Q(H) c [s $^{-1}$]	N(OB) d	$\mathcal{M}_{\text{tot}}^e$ [M $_{\odot}$]
A194S	Total	−21.05	5.7×10^{41}	4.5	4.8×10^{53}	100000	1.8×10^7
A194S	A Nucleus	−19.91	2.0×10^{41}	1.6	1.7×10^{53}	34000	6.3×10^6
A194	Blob A	−17.88	1.6×10^{41}	1.2	1.3×10^{53}	27000	5.0×10^6
A194	Blob B	−18.04	5.4×10^{40}	0.4	4.6×10^{52}	9000	1.7×10^6
A194	Blob C	−18.24	3.5×10^{40}	0.3	3.0×10^{52}	6000	1.1×10^6
A194N	Total	−21.85	3.4×10^{41}	2.7	2.9×10^{53}	60000	1.1×10^7
A194N	A “Nucleus”	−19.11	5.3×10^{40}	0.4	4.5×10^{52}	9000	1.7×10^6
A194N	B	−18.19	3.4×10^{40}	0.3	2.9×10^{52}	6000	1.1×10^6
A194N	Blob D	−18.18	... ^f
A194N	Arc Spot A	−17.97	2.7×10^{40}	0.2	2.3×10^{52}	5000	8.7×10^5
A194N	Arc Spot B	−18.26	1.8×10^{40}	0.15	1.5×10^{52}	3000	5.7×10^5
A194N	Arc Spot C	−18.19	2.4×10^{40}	0.2	2.0×10^{52}	4000	7.63×10^5

^aBlue absolute magnitude M_B .

^bTotal SFR from 0.1 to 100 M $_{\odot}$ computed for a Salpeter IMF from L(H α): SFR $\approx 7.9 \times 10^{-42}$ L(H α) M $_{\odot}$ yr $^{-1}$ (Kennicutt 1998).

^cThe number of ionizing photons Q(H) has been computed from L(H α) following case B of nebular theory, assuming T $_e \approx 10000^\circ$ K, and no photon escaping the nebula.

^dNumber of OB stars, i.e., stars in the mass range 10 M $_{\odot}$ – 100 M $_{\odot}$, computed from Q(H) assuming a relationship between each star Q(H) and mass from Kurucz’s models (A. Bressan, private communication), and a Salpeter IMF.

^eTotal mass of IMF stars from 0.1 M $_{\odot}$ to 100 M $_{\odot}$ assuming a Salpeter IMF.

^fVery faint H α emission.

REFERENCES

- Amram, P., Mendes de Oliveira, C., Boulesteix, J., & Balkowski, C. 1998, *A&A*, 330, 881.
- Appleton, P. N. & Marston, A. P. 1997, *AJ*, 113, 201.
- Appleton, P.N., Schombert, J.M., Robson, E.I., 1992, *ApJ* 385, 491
- Appleton, P.N., Struck-Marcell, C., 1987, *ApJ* 318, 103
- Arp, H. 1966, *ApJS*, 14, 1.
- Barnes, J. E. & Hernquist, L. 1992, *Nature*, 360, 715.
- Barnes, J. E. & Hernquist, L. 1996, *ApJ*, 471, 115.
- Barnes, J. E. & Hernquist, L. 1998, *ApJ*, 495, 187.
- Baum, S. A. & Heckman, T. 1989, *ApJ*, 336, 702.
- Becker, R. H., White, R. L., & Helfand, D. J. 1995, *ApJ*, 450, 559.
- Bressan, A., Silva, L., & Granato, G. L. 2002, *A&A*, 392, 377
- Bushouse, H. A. & Stanford, S. A. 1992, *ApJS*, 79, 213
- Charmandaris, V., Laurent, O., Mirabel, I.F., Gallaris, P., Sauvage, M., Vigroux, L., Cesarsky, C., 2001, *ApSS* 276, 553
- Clark, D. H. & Caswell, J. L. 1976, *MNRAS*, 174, 267.
- Colina, L., Alberdi, A., Torrelles, J. M., Panagia, N., & Wilson, A. S. 2001, *ApJ*, 553, L19.
- de Mello, D. F., Keel, W. C., Sulentic, J. W., Rampazzo, R., Bica, E., & White, R. E. 1995, *A&A*, 297, 331.
- de Mello, D. F., Sulentic, J. W., de Souza, R. E., Reduzzi, L., & Rampazzo, R. 1996, *A&A*, 308, 387.
- Domingue, D. L. 2001, Ph.D. Thesis, The University of Alabama
- Duc, P.A., Brinks, E., Springel, V., Pichardo, B., Weilbacher, P., Mirabel, I.F., 2000, *AJ* 120, 1238
- Duc, P.-A., Brinks, E., Wink, J. E., & Mirabel, I. F. 1997, *A&A*, 326, 537.
- Dultzin-Hacyan, D. 1995, *Revista Mexicana de Astronomia y Astrofisica Conference Series*, 3, 31.
- Fraternali, F., Oosterloo, T., Sancisi, R., & van Moorsel, G. 2001, *ApJ*, 562, L47.
- Gerber, R. A., Lamb, S. A., & Balsara, D. S. 1992, *ApJ*, 399, L51.

- Hattori, T., Yoshida, M., Ohtani, H., Ishigaki, T., Sugai, H., Hayashi, T., Ozaki, S., & Ishii, M. 2002, PASJ, 54, 393
- Hearn, N. C. & Lamb, S. A. 2001, ApJ, 551, 651.
- Heckman, T. M. 2001, To appear in "Extragalactic Gas at Low Redshift", ed. J. Mulchaey & J. Stocke, ASP Conf. Series, 7438.
- Heckman, T. M., Lehnert, M. D., & Armus, L. 1993, ASSL Vol. 188: The Environment and Evolution of Galaxies, 455.
- Ho, L. C. & Ulvestad, J. S. 2001, ApJS, 133, 77.
- Horellou, C. & Combes, F. 2000, ASP Conf. Ser. 197: Dynamics of Galaxies: from the Early Universe to the Present, 351.
- Keel, W. C. 2000, American Astronomical Society Meeting, 197,# 37.01
- Kennicutt, R. 1983, A&A, 120, 219
- Kennicutt, R. C. 1998, ARA&A, 36, 189.
- Krongold, Y., Dultzin-Hacyan, D., Marziani, P. 2002, ApJ, in press.
- Lynds, R. & Toomre, A. 1976, ApJ, 209, 382.
- Maiolino, R., Vanzi, L., Mannucci, F., Cresci, G., Ghinassi, F., & Della Valle, M. 2002, astro-ph/0204107, accepted for publication in A&A.
- Marston, A.P., Appleton, P.N., 1995, AJ 109, 1002
- Marziani, P., D'Onofrio, M., Dultzin-Hacyan, D. & Sulentic, J. W. 1999, AJ, 117, 2736
- Marziani, P. & Dultzin-Hacyan, D. 2000, ASP Conf. Ser. 215: Cosmic Evolution and Galaxy Formation: Structure, Interactions, and Feedback, 122.
- Marziani, P., Keel, W. C., Dultzin-Hacyan, D. & Sulentic, J. W. 1994, ApJ, 435, 668
- Metlov, V. G. 1980, Soviet Astronomy Letters, 6, 110.
- Mihos, J. C. & Hernquist, L. 1996, ApJ, 464, 641.
- Mioduszewski, A. J., Dwarkadas, V. V., & Ball, L. 2001, ApJ, 562, 869
- Osterbrock, D. E. 1989, in Astrophysics of gaseous nebulae and active galactic nuclei, Mill Valley CA, University Science Books
- Owen, F. N., Spanger, S. R., & Cotton, W. D. 1980, AJ, 85, 351

- Persic, M. & Salucci, P. 1995, *ApJS*, 99, 501.
- Phillips, A. C. 1993, *AJ*, 105, 486.
- Rafanelli, P. & Marziani, P. 1992, *AJ*, 103, 743.
- Rubin, V. C., Thonnard, N., & Ford, W. K. 1980, *ApJ*, 238, 471.
- Sanders, D. B. & Mirabel, I. F. 1996, *ARA&A*, 34, 749
- Sanders, D. B., Soifer, B. T., Elias, J. H., Neugebauer, G., & Matthews, K. 1988, *ApJ*, 328, L35.
- Schmitt, H. R. 2001, *AJ*, 122, 2243.
- Semelin, B. & Combes, F. 2000, *A&A*, 360, 1096.
- Smith, B.J., Wallin, J.F., 1992, *ApJ* 393, 544
- Smith, B.J., Struck, C., Pogge, R.W., 1997, *ApJ* 483, 754
- Struck-Marcell, C., 1990, *AJ* 99, 71 Struck, C., 1997, *ApJSS* 113, 269
- Theys, J.C., Spiegel, E.A., 1976, *ApJ* 208, 650
- Toomre, A., 1978, in “The Large Scale Structure of the Universe”, *IAU Symp.* 79, M.S. Longair and J. Einasto (eds), Reidel, Netherlands, p. 109
- Ulvestad, J. S. 1982, *ApJ*, 259, 96.
- Ulvestad, J. S. & Ho, L. C. 2001, *ApJ*, 558, 561.
- van der Hulst, T. & Sancisi, R. 1988, *AJ*, 95, 1354.
- Veilleux, S. & Osterbrock, D. E. 1987, *ApJS*, 63, 295.
- Vorontsov-Vel’Yaminov, B. A. 1977, *A&AS*, 28, 1.
- Yin, Q. F. & Heeschen, D. S. 1991, *Nature*, 354, 130.
- Wakker, B. P. & van Woerden, H. 1997, *ARA&A*, 35, 217.
- Walker, I. R., Mihos, J. C., & Hernquist, L. 1996, *ApJ*, 460, 121.

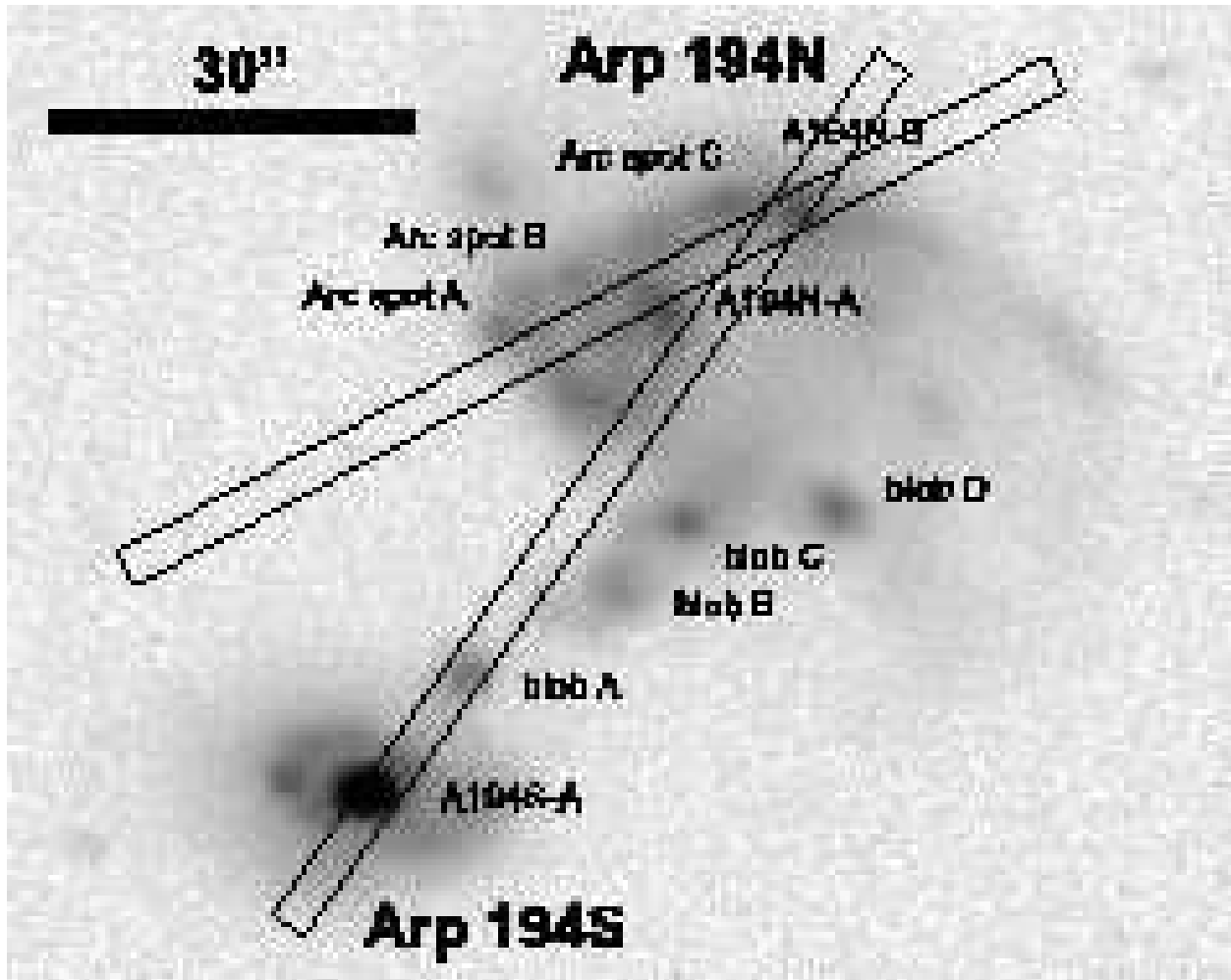


Fig. 1.— Morphological details of the Arp 194 system and their identification. The slit position (P.A. = 145° and P.A. = 118°) and width ($2.6''$) is shown on scale. North is to the top and East is to the left. Uncertainty in the placement of the slit is estimated to be within $\pm 0.5''$

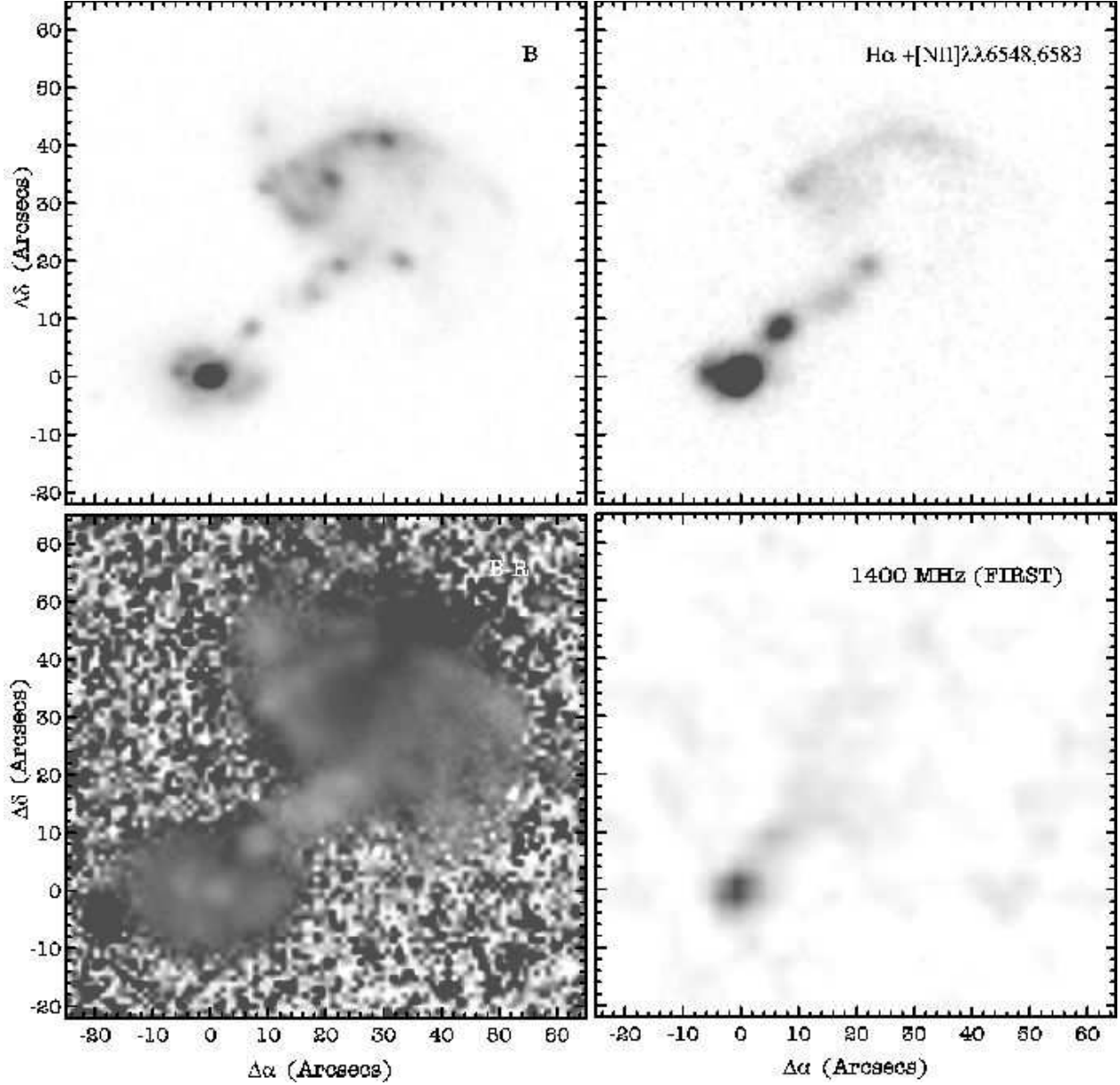


Fig. 2.— Multifrequency morphology of the Arp 194 system. Upper left panel: Johnson B image. Upper right panel: Continuum-subtracted narrow band image [H α + [NII] $\lambda\lambda$ 6548,6583]. Lower left panel: $B - R$ color map. Limits on scale are -1.2 (white) and 1.2 (black). Lower right panel: radio emission at 1.4 GHz from FIRST data. In all panels, North is to the top and East is to the left.

Arp 194 P. A. = 145

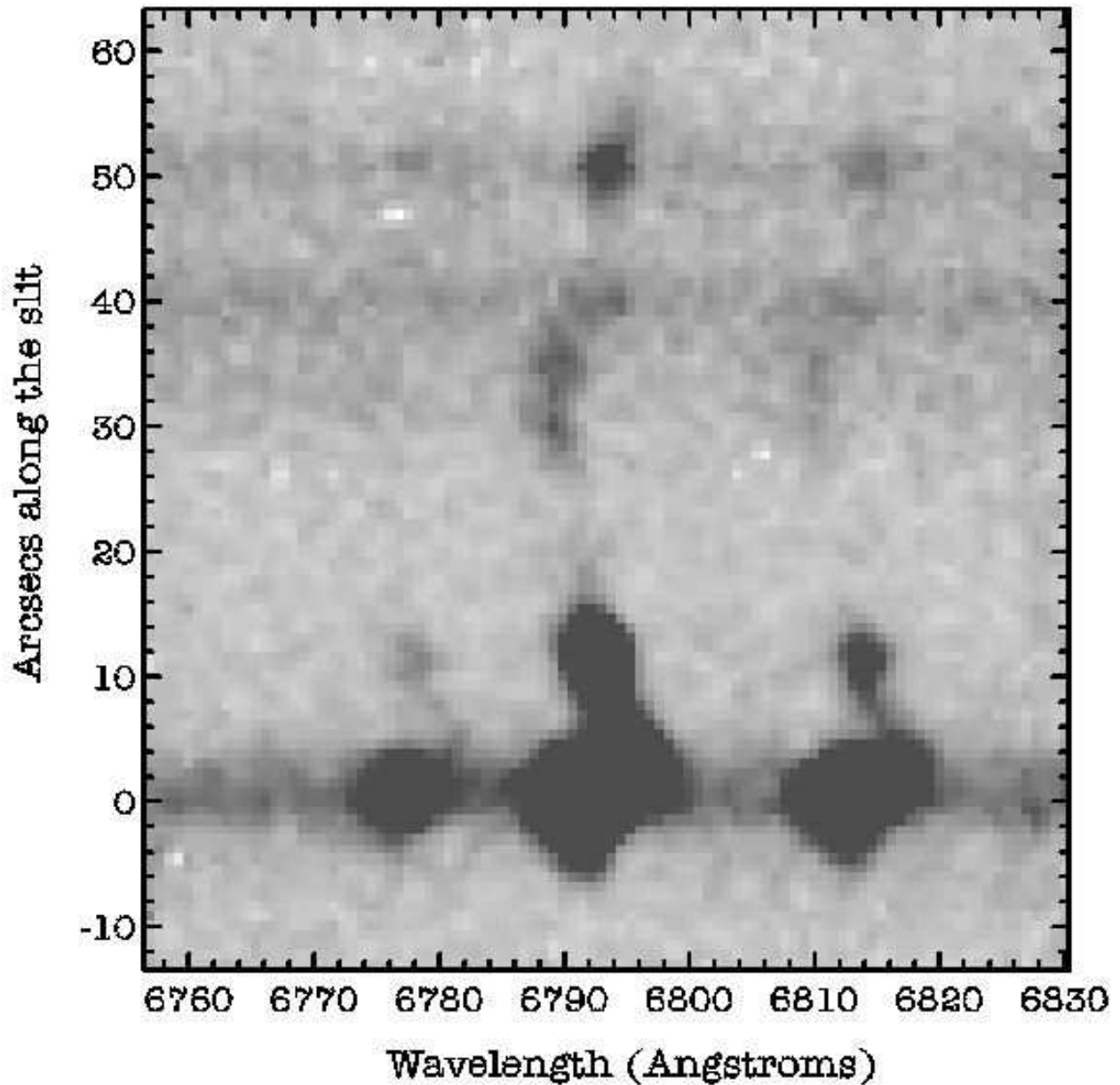


Fig. 3.— Long slit spectrum of Arp 194, at P. A. $\approx 145^\circ$, in the range covering $H\alpha$ and $[NII]\lambda\lambda 6548, 6583$. Abscissa is observed wavelength in \AA ; ordinate is arcsec along the slit (NW to the top). The light contour levels are meant to emphasize the line structure in the inner few arcsecs of A194S.

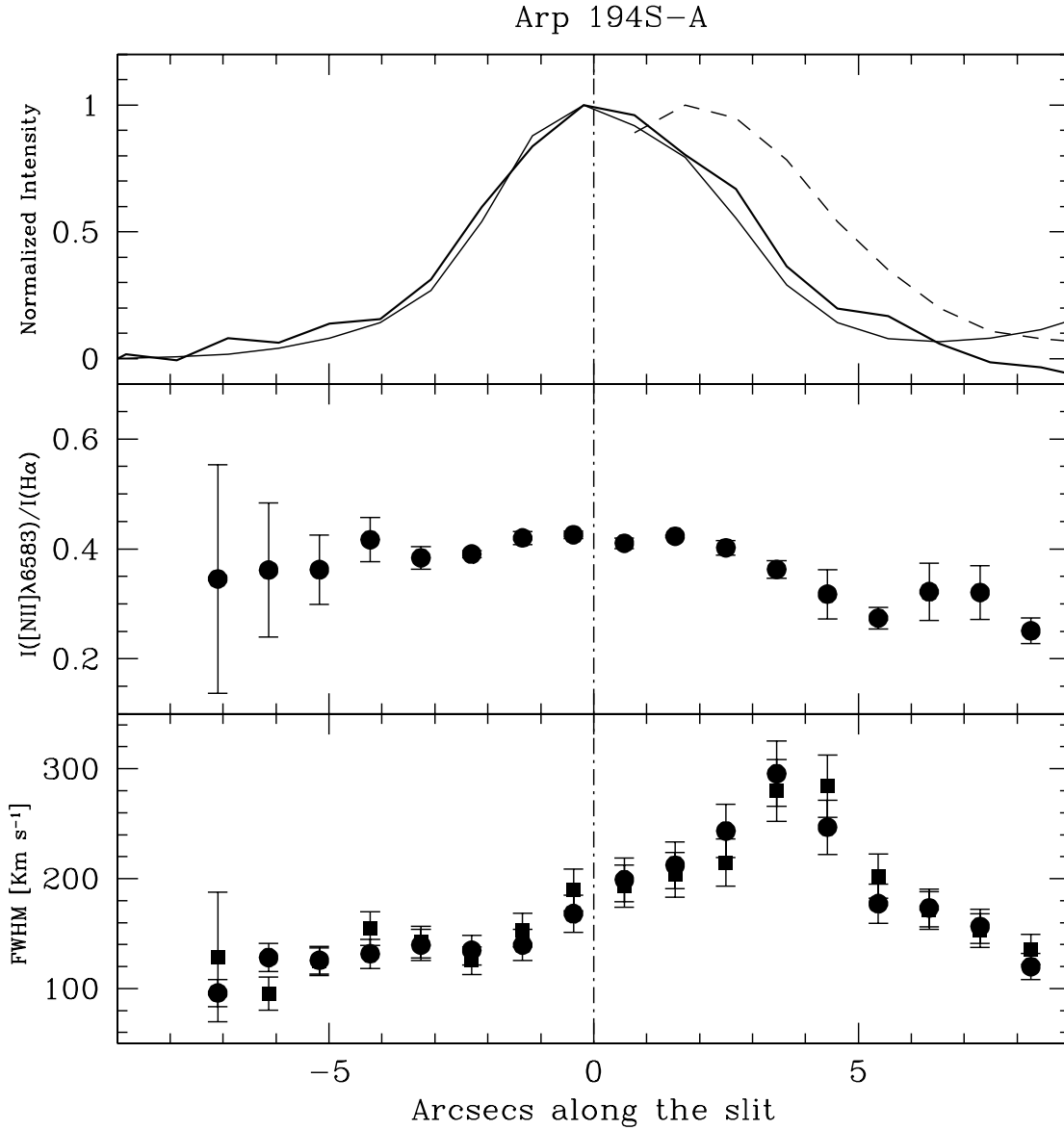


Fig. 4.— Upper panel: cross dispersion intensity profile for H α emission (thin solid line), continuum (thick solid line; assumed to peak at the abscissa 0 point), and extended H α component (dashed line). Ordinate is intensity normalized to peak value. The extended H α component peaks approximately 2'' from the continuum, and it is barely visible in the strip of maximum continuum emission (see also 3). Middle panel: Intensity ratio of the H α and [N II] λ 6583 lines, as a function of the distance from the nucleus of A194S. Lower Panel: for FWHM(H β) (filled circles) and FWHM([N II] λ 6583) (filled squares) vs. distance from the nucleus of A194S. Ordinate is FWHM in km s $^{-1}$ corrected for instrumental profile.

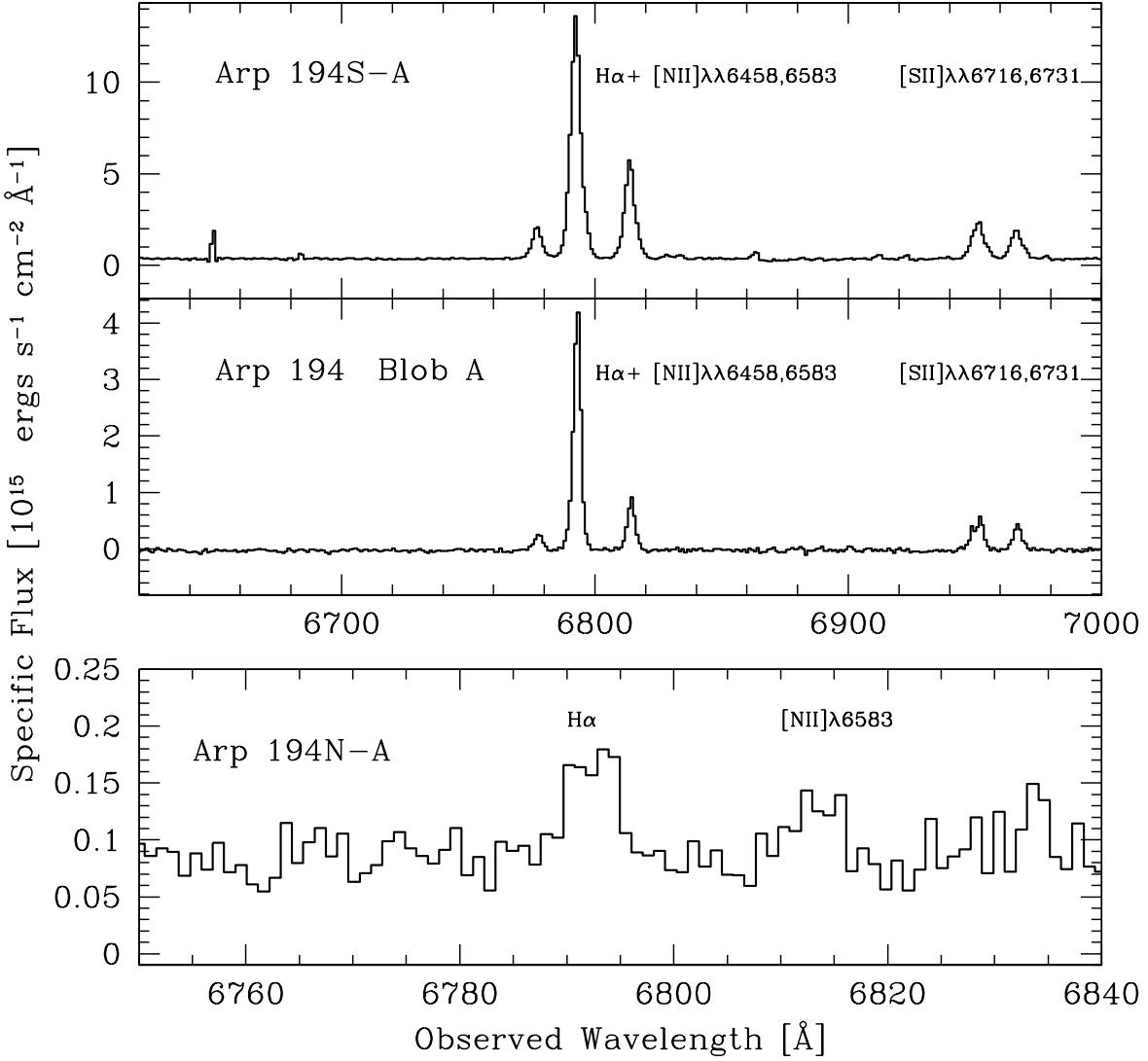


Fig. 5.— H α spectral regions of relevant emitting line regions, ordered from the South to the North. Abscissa is observed wavelength in \AA , ordinate is specific flux in units of $\text{ergs s}^{-1} \text{ cm}^{-2} \text{ \AA}^{-1}$. The A194N-A spectrum (bottom panel) spectral range has been expanded, to better show the boxy and broad appearance of H α .

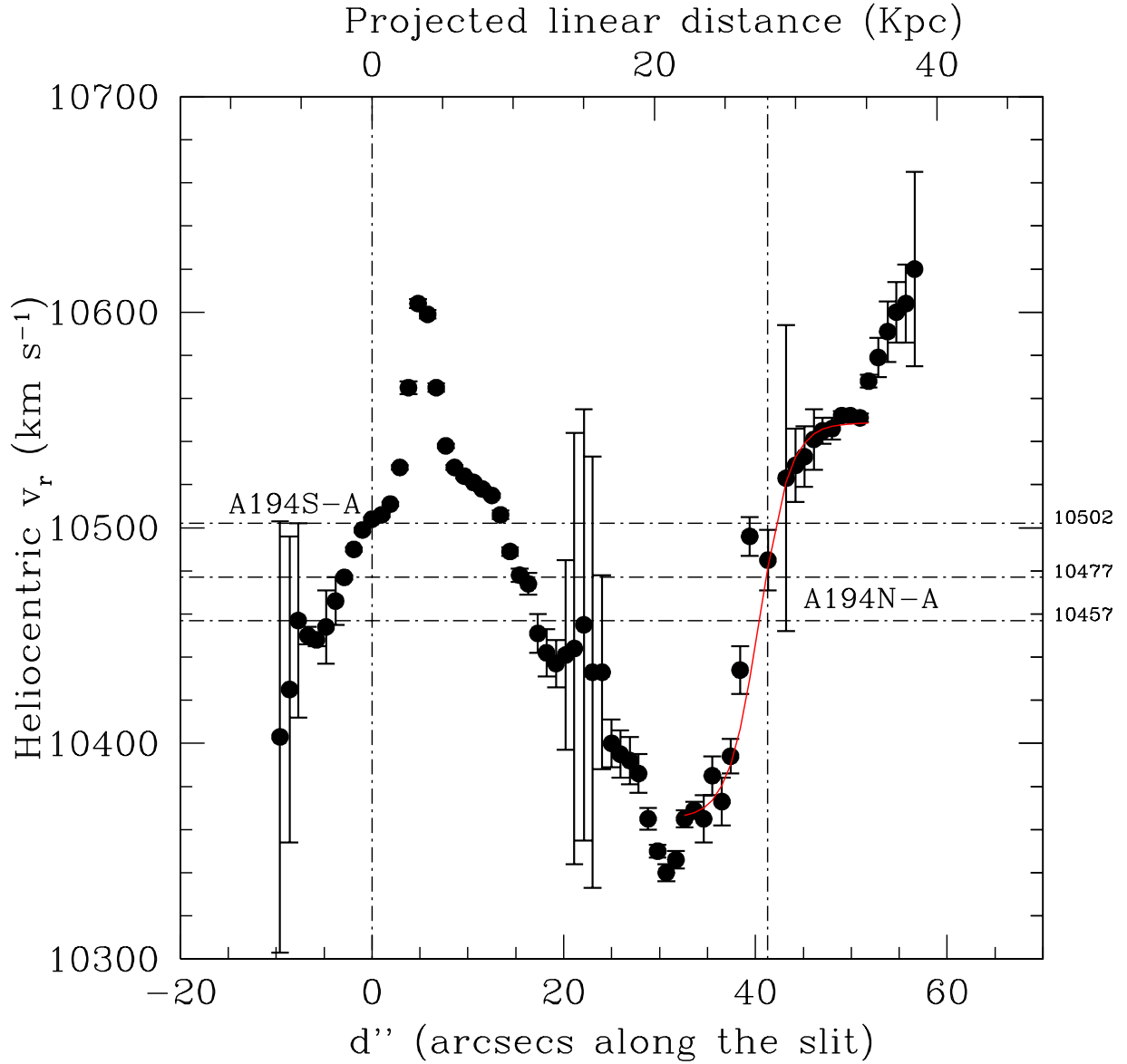


Fig. 6.— Heliocentric radial velocity curve of the Arp 194 system at P. A. = 145°. Note that the apparent discordant point at $\approx 40''$ reflects a broadening of the H α and [NII] $\lambda\lambda 6548, 6583$ lines. The origin of the projected linear and angular distance scale has been set coincident with A194S-A (at cross-dispersion peak of the continuum). The three dot-dashed lines draw the systemic v_r measured for A194S ($v_r \approx 10502$ km s $^{-1}$) and A194N ($v_r \approx 10457$ km s $^{-1}$ and 10477 km s $^{-1}$; see text for details).

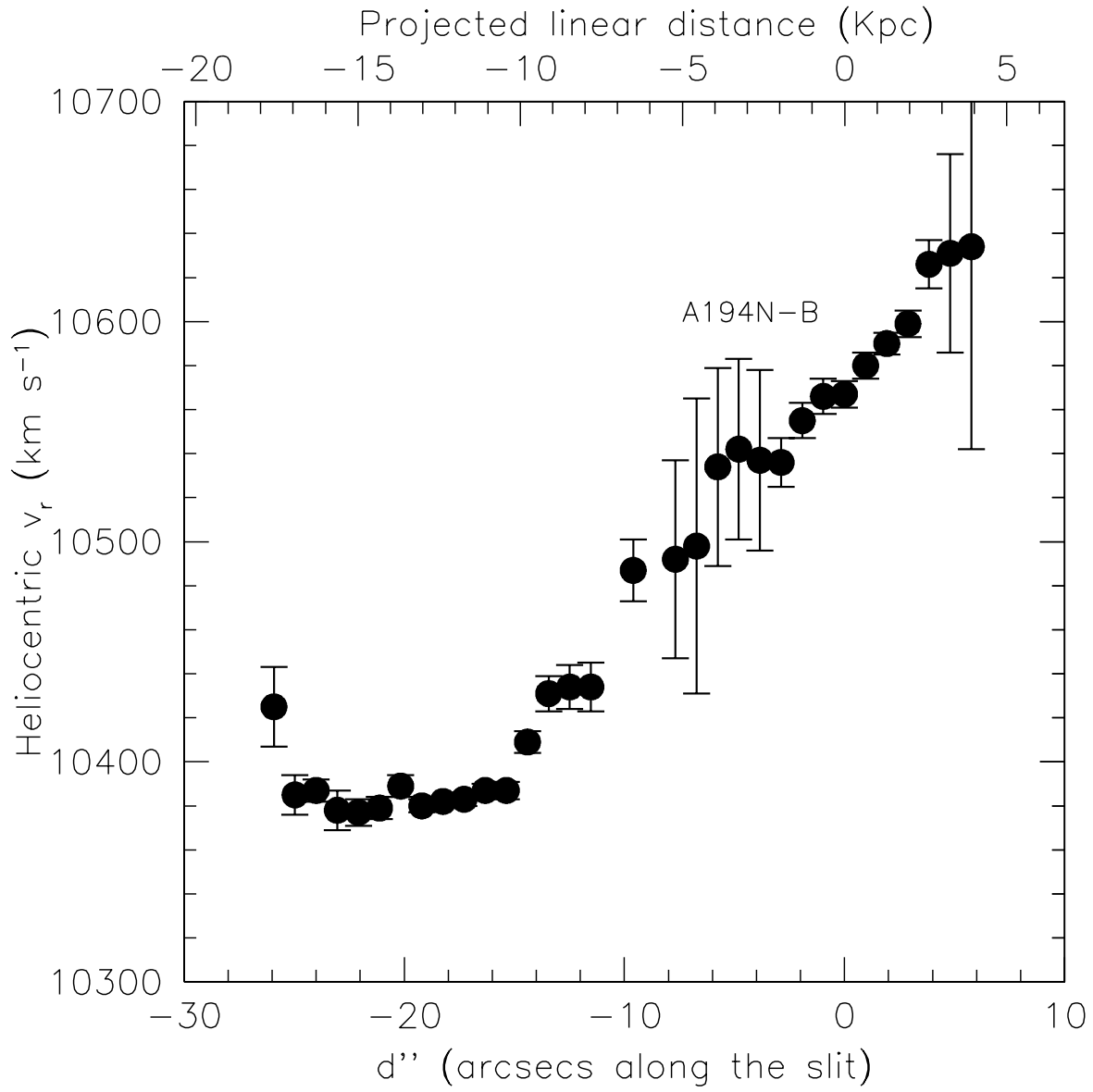


Fig. 7.— Heliocentric radial velocity curve of the Arp 194 system at P. A. = 118° . Note that, at variance with the previous figure, the origin has been set on A194N-B.

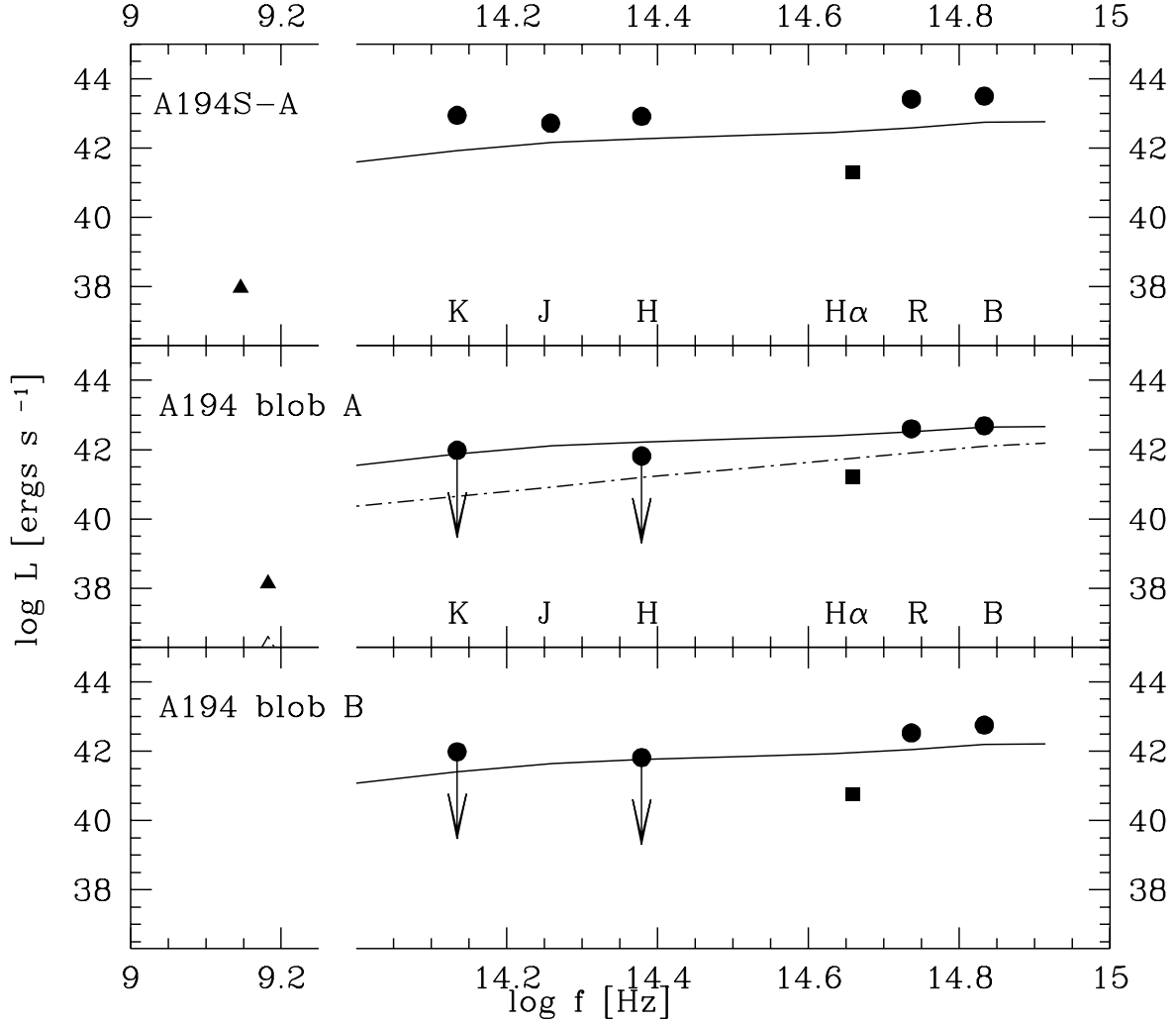


Fig. 8.— Photometric properties of A194S-A, blob A and blob B and population synthesis. Abscissa is logarithm of frequency in Hertz, ordinate is logarithm of νL_ν in ergs s^{-1} . The filled squares represent the $\text{H}\alpha$ luminosity. The solid line shows the prediction of STARBURST99 simulations for the continuous SFR as reported in the 4th column of Table 5: $1.55, 1.2, 0.42 \text{ M}_\odot \text{yr}^{-1}$ for A194S-A, blob A and blob B respectively, after a time $\approx 7 \times 10^7 \text{ yr}$. Errors are approximately the size of the symbols or smaller. The dot-dashed line of the middle panel is a simulation for the “first generation of stars” hypothesis (see text) with a main sequence total mass $\mathcal{M}_{\text{tot}} \approx 5 \times 10^6 \text{ M}_\odot$. The triangle refer to the expectation for radio power in case of only free-free emission. No correction for external extinction has been applied.